

Time-Resolved X-, K-, and W-Band EPR of the Radical Pair State $P_{700}^{+}A_1^{-}$ of Photosystem I in Comparison with $P_{865}^{+}Q_A^{-}$ in Bacterial Reaction Centers

A. van der Est,^{*,†} T. Prisner,[†] R. Bittl,[‡] P. Fromme,[‡] W. Lubitz,[‡] K. Möbius,[†] and D. Stehlik[†]

Fachbereich Physik, Freie Universität Berlin, Arnimallee 14, 14195 Berlin, Germany, and Max Volmer Institut, Technische Universität Berlin, Strasse des 17. Juni 135, 10623 Berlin, Germany

Received: July 22, 1996; In Final Form: November 15, 1996[⊗]

The spin-polarized EPR spectra at 95 GHz (W-band), 24 GHz (K-band), and 9 GHz (X-band) of the radical pair $P_{700}^{+}A_1^{-}$ in highly purified photosystem I particles are presented. The spectra are analyzed to obtain both the magnetic parameters of the radical pair as well as the relative orientation of the two species. From the analysis, the g -tensor of A_1^{-} is found to be $g_{xx} = 2.0062$, $g_{yy} = 2.0051$, and $g_{zz} = 2.0022$, and it is shown that A_1 is oriented such that the carbonyl bonds are parallel to the vector joining the centers of P_{700}^{+} and A_1^{-} . The anisotropy of the g -tensor is considerably larger than that obtained for chemically reduced phyloquinone in frozen 2-propanol solution. Possible reasons for this difference and their implications for the A_1 binding site are discussed. The relative orientation of P_{700}^{+} and A_1^{-} is compared with earlier estimates obtained using less accurate g -values for A_1^{-} . A comparison with the spectra of $P_{865}^{+}Q_A^{-}$ in bacterial reaction centers (bRCs) of *Rhodobacter sphaeroides* R-26 in which the nonheme iron has been replaced by zinc (Zn-bRCs) allows the structural and magnetic properties of the charge-separated state in the two systems to be compared. From the similarity of the two W-band spectra in the region around the free electron g -value it is clear that the dipolar vector, z_d , between P^{+} and Q_A^{-}/A_1^{-} has a similar orientation relative to P_{700} in PS I and P_{865} in bRCs. This is compatible with the similar overall structural arrangement of P_{700} and P_{865} . In contrast, the low-field parts of the two spectra are very different as a result of differences in the orientation of A_1 and Q_A with respect to z_d .

Introduction

The charge-separated radical pair states $P_{700}^{+}A_1^{-}$ and $P_{865}^{+}Q_A^{-}$ generated by the light-induced electron transfer in photosystem I (PS I) and reaction centers of purple bacteria (bRCs), respectively, have been studied extensively using transient EPR (for reviews see for example refs 1, 2). The spectra of these states are spin polarized and contain structural information about the spin system. In particular, the geometry of the radical pair can be deduced from the polarization pattern because the magnetic interactions in the system are tensorial. The EPR data also provide a way of probing the interaction of the donor, P, and the quinone acceptor with the protein matrix because the g -tensor and hyperfine couplings of the two radical ions are influenced by their local surroundings. This is of special interest in the case of the quinones Q_A and A_1 because their properties should reflect the fact that the subsequent acceptors are different in bRCs and PS I.

In native bRCs, the interpretation of the transient EPR spectra is complicated by the fact that Q_A is strongly coupled to the high-spin nonheme iron, Fe^{2+} . However, this problem can be avoided by substituting the iron with diamagnetic zinc, Zn^{2+} . The spectra of such samples^{1,3–6} can be calculated⁴ essentially without adjustable parameters if the X-ray structure of the ground state is used. The agreement between the calculations and the experimental spectra indicates that, within experimental error, the orientation of the radical ions in the charge-separated state in frozen solution is the same as that of the corresponding neutral molecules in the ground state in single crystals at room

temperature. At present, such conclusions are limited by the accuracy of the X-ray structure, which has a resolution⁷ of 2.65 Å.

In PS I the situation is less clear because the structure of the ground state is not known in sufficient detail. The most recent electron density map⁸ at 4.5 Å resolution obtained from PS I single crystals suggests a fairly high degree of homology between the structure of the PS I RC and that of purple bacteria in the region of the primary donor, P_{700} . The positions and orientations of the other cofactors appear to become increasingly different the further away they are from P_{700} . In particular, the location and orientation of A_1 cannot be deduced from the data. In principle, this information can be obtained from the transient EPR spectra of $P_{700}^{+}A_1^{-}$, which depend on the relative orientation of the g -tensors of the two radicals and the vector z_d , which characterizes the dipolar coupling and joins the centers of P^{+} and A_1^{-} . Thus, if the principal axes of the g -tensors can be assigned to the respective molecular axes, the relative orientation of cofactors can be determined. In addition, the center to center distance between the radicals can be calculated from the magnitude of the dipolar coupling constant on the basis of the well-justified, point-dipole approximation.

The molecular orientation for A_1^{-} , with the carbonyl bonds roughly parallel to the vector joining P_{700}^{+} and A_1^{-} , was obtained⁹ from simulations of the K-band (24 GHz) and X-band (9 GHz) transient EPR spectra of perdeuterated PS I and was substantiated in further studies.³ A qualitatively similar but different quinone orientation has been suggested from an analysis of the quantum beats observed in the X-band EPR transients.^{10,11}

In another study,¹² a comparison was made of PS I and Zn-bRC samples in which the respective native quinones phyloquinone (vitamin K₁, VK1) and ubiquinone-10 (UQ) were

* To whom correspondence should be addressed.

† Freie Universität.

‡ Technische Universität.

⊗ Abstract published in *Advance ACS Abstracts*, January 15, 1997.

replaced by duroquinone (DQ) and naphthoquinone (NQ). The remarkable result of this comparison is that the behavior of the quinones in the two RCs is quite different. In Zn-bRCs, UQ, NQ, and DQ have roughly the same orientation, whereas in PS I large differences in the orientations of VK1, NQ, and DQ were found. In addition, the *g*-anisotropy of the quinones is influenced by their surroundings and is larger in PS I. These results can be understood if one assumes that the binding between the quinone and the protein in PS I is weaker than in bRCs.

The majority of the published transient EPR data on photosynthetic reaction centers have been measured at a microwave frequency of 9 GHz (X-band).¹ At this frequency the spectral features of the *g*-tensor components of the radicals overlap to a large extent and are obscured by the hyperfine couplings. On one hand, this makes the spectra very sensitive to small changes in the geometry; on the other hand, it creates severe difficulties in finding a unique and reliable set of parameters that describe them. To overcome this problem, the relative influence of magnetic field independent interactions, such as the hyperfine couplings, can be reduced by working at higher microwave frequencies and/or deuterating the sample. In the studies mentioned above, the improved spectral resolution obtained by deuteration and at 24 GHz (K-band) is crucial for extracting structural information from the data. It has now become possible to do such experiments at considerably higher microwave frequency, and recently we reported the first spin-polarized W-band (95 GHz) spectra of $P_{865}^{+}Q_A^{-}$ in both protonated and deuterated Zn-bRCs.⁵ The improved resolution reduces the dependence on deuterated samples, which can in principle have different structural properties compared to native systems. The W-band spectra are simulated well using only parameters obtained from independent experimental results and taking the hyperfine couplings into account as an inhomogeneous linewidth. The fact that the agreement becomes progressively worse with decreasing Zeeman energy and with protonated samples, i.e. as the relative importance of the hyperfine couplings in the spectra increases, clearly demonstrates that successful simulation of X-band spectra requires proper consideration of the hyperfine couplings. Obviously this will work best if the field dependent parameters can be determined from accompanying measurements at sufficiently high field at which the hyperfine couplings contribute at most to the linewidth.

Here, we will present X-, K-, and W-band spectra of $P_{700}^{+}A_1^{-}$ in highly purified PS I preparations from *Synechococcus elongatus*, from which the first PS I electron density maps have been determined.^{8,13} Since differences exist between the spectra of different species under different conditions, the spectra have been measured on one sample under the same conditions. The set of three spectra allow an accurate determination of the *g*-tensor of A_1^{-} , which we find to have a considerably larger anisotropy compared to phyloquinone in frozen 2-propanol. We will discuss possible reasons for this in terms of the interaction of A_1 with its binding site. We will then determine the relative orientation of P_{700}^{+} and A_1^{-} from simulations of the polarization patterns using as much independent information as possible. In particular, we will use the values of the dipolar and exchange couplings obtained from out-of-phase spin echo experiments,^{14,15} which are considerably different from previous estimates^{9,10} for PS I. We will compare the results to the geometries^{9,10} obtained using less accurate *g*-values and couplings. We will also compare the spectra of $P_{700}^{+}A_1^{-}$ with those of $P_{865}^{+}Q_A^{-}$ in Zn-bRCs from *Rhodobacter sphaeroides* R-26^{3,5} and discuss the similarities and differences with respect to the structure and cofactor binding in the two systems.

Materials and Methods

PS I Samples. PS I was isolated from the thermophilic cyanobacterium *S. elongatus* using a method similar to that described in ref 16, which will be described in detail elsewhere.¹⁷ To reduce possible effects due to heterogeneity in the PS I particles, the EPR samples were prepared by dissolving crystals of PS I. These crystals are identical to those used for X-ray analysis,⁸ where no heterogeneity of the protein is observed. PS I is isolated and crystallized in trimeric form with a molecular mass of 1020 kDa. The PS I monomers are composed of 11 protein subunits (PsaA...PsaF, PsaI...PsaM), each of which occurs once per reaction center. In addition, the monomers contain 20 carotenoid and about 100 chlorophyll *a* molecules per P_{700} .

Twenty milligrams of wet PS I crystals grown at low salt concentrations¹⁸ were dissolved in 20 μ L of buffer (5 mM MES, pH 6.4, 100 mM $MgSO_4$, 0.02% β -dodecylmaltoside). The final chlorophyll concentration was 20 mM, corresponding to a protein concentration of 80 mg/mL. To remove any oxidized P_{700} present, sodium ascorbate was added to the solution, which was then transferred to a quartz capillary (o.d. \sim 0.9 mm), mounted in the W-band cylindrical TE_{011} cavity, and frozen in the dark.

Zn-bRC Samples. The preparation of Zn-substituted reaction centers of *R. sphaeroides* is described in ref 3, and the details of the time-resolved EPR experiments at various frequencies on these samples are given elsewhere.^{3,5}

EPR Experiments. The home-built pulsed W-band EPR spectrometer has been described previously,¹⁹ as have the details of the transient nutation and spin echo experiments.^{5,20} The X-band²¹ and K-band²² spectrometers are also described in the literature.

Measurement of $P_{700}^{+}A_1^{-}$ at Low Temperature. In PS I the charge separation from P_{700} to the terminal iron-sulfur centers F_A/F_B is irreversible at low temperatures. In principle, this implies that after a number of flashes all reaction centers will be in the state $P_{700}^{+}(F_A/F_B)^{-}$ and no further electron transfer can be generated by additional flashes. However, it has been reported²³ that at 10 K charge recombination from A_1^{-} occurs in a fraction of the centers. A more detailed investigation of the temperature dependence of the light-induced absorbance changes in PS I²⁴ showed that this fraction is strongly temperature dependent and that below 77 K stable reduction of F_A/F_B occurs in only about 35% of the centers. The lifetime of $P_{700}^{+}A_1^{-}$ is also strongly temperature dependent. At room temperature it is approximately 200 ns^{25,26} and is limited by the electron transfer to F_X .²⁷⁻²⁹ Below 77 K, forward electron transfer beyond A_1^{-} is blocked in about 65% of the centers, and under these conditions the lifetime of $P_{700}^{+}A_1^{-}$ is $t_{1/2} \approx 200 \mu$ s. This means that, in low-temperature time-resolved EPR experiments, both a stationary spectrum primarily due to P_{700}^{+} and a spin-polarized spectrum due to $P_{700}^{+}A_1^{-}$ are observed. In the X- and K-band transient EPR experiments presented here, the P_{700}^{+} spectrum is detected as a time independent background, which is subtracted when the digital boxcar spectra are extracted from the full time/field data sets.^{3,9} In a spin echo experiment both signals from the two species overlap. Thus, to separate them, a light minus dark difference must be taken. Alternatively, the P_{700}^{+} echo signal can be suppressed by applying a series of microwave pulses before the laser flash. In the W-band spectra presented here, the field-swept echo detected spectrum was first collected with the microwave pulse sequence being applied directly after the laser flash. The experiment was then repeated, but with the microwave pulses placed in such a

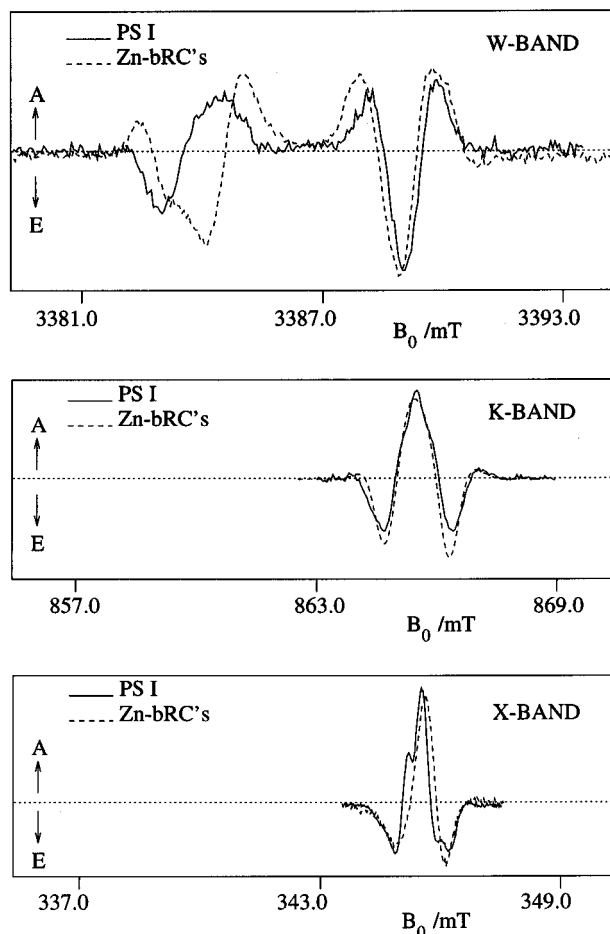


Figure 1. Comparison of spin-polarized EPR spectra of $P_{700}^+A_1^-$ in PSI and of $P_{865}^+Q_A^-$ in Zn-bRCs at three different microwave frequencies (from top to bottom 95, 24, and 9 GHz): solid curve, PS I; dashed curve, Zn-bRC; W-band, two-pulse field-swept echo spectra (see text) microwave frequency (ν_{MW}) 95.462 GHz, $T = 150$ K; K-band, digital boxcar transient nutation spectra 50–300 ns following the laser flash; $\nu_{MW} = 24.269$ GHz, $T = 50$ K; X-band, digital boxcar transient nutation spectra 300–400 ns after laser flash; $\nu_{MW} = 9.706$ GHz, $T = 77$ K (bRCs), $T = 150$ K (PS I).

way that the echo was detected just before the laser flash. It is the difference of the two spectra that is presented here (see below).

Magnetic Field Calibration. It is important for the magnetic field to be calibrated because we are interested in extracting accurate g -values from the spectra. As described in ref 5, the spin-polarized spectra were measured together with a Mn^{2+} standard using the spin-echo method. Because Mn^{2+} has a much shorter T_2 relaxation time than $P_{700}^+A_1^-$ and $P_{865}^+Q_A^-$, the radical pair spectrum can be recorded with or without that of the standard by varying the delay between the two microwave pulses. The calibration of the field in the X- and K-band experiments is described in ref 12.

Results and Spectral Simulations

Experimental Spectra. In Figure 1, the W-band two-pulse echo detected spectrum and the X- and K-band transient nutation spectra of $P_{700}^+A_1^-$ from the same PS I preparation in frozen solution are shown along with the corresponding spectra of $P_{865}^+Q_A^-$.⁵ This figure clearly demonstrates the importance of performing such experiments at various microwave frequencies. At X- and K-band, the spectra of the two RCs have the same general shape, although subtle differences between them can be seen. Some of these differences, which become more pronounced with deuterated samples, have been analyzed in

terms of the quinone orientation in the two systems.³ At W-band, the spectra of the protonated samples are well resolved and the differences become much clearer and readily interpretable. The W-band spectra can be divided into two regions, which we will refer to as the high-field and low-field parts. The most striking feature in the comparison of the two spectra is that the patterns are very similar in the high-field part, whereas they are very different in the low-field region. The latter is due to transitions associated mainly with the flip of the unpaired electron spin on the quinone acceptor, whereas the high-field features are primarily due to transitions associated with the oxidized donor P^{*+} . Strictly speaking, both spins of the radical pair are involved in all transitions; however, the assignment of parts of the spectra to individual species is a very good approximation when the difference in the resonance frequencies, $\Delta\omega$, of two radical spins is large compared to the coupling between them. (For the low-field region, $\Delta\omega$ is about 50 times larger than the coupling, which is ~ 3 MHz.) As has been demonstrated in several publications,^{1,3,6,9,10,30,31} the polarization patterns in the two regions of the spectra are determined primarily by the relative orientation of the g -tensor axes and the dipolar vector, z_d . Thus, the similarity of the high-field parts of the spectra in Figure 1 suggests that the orientation of z_d relative to the donor g -tensor is roughly the same in both systems. In contrast, the very different low-field parts clearly show that the quinones in the two RCs are oriented differently, as was inferred from the less pronounced spectral evidence at lower frequencies.^{3,12} The good spectral resolution at W-band frequencies allows the orientation of the individual g -tensor axes to be estimated by inspection. Such a qualitative analysis helps with the initial parameter choice for the simulations and provides a better understanding of the results.

Qualitative Description of the Spectra. For a given orientation of the radical pair the spectrum consists of two pairs of oppositely polarized lines: one pair associated with P^{*+} and the other with $Q^{\bullet-}$. At W-band the coupling between the unpaired spins is small compared to the difference in the resonance frequencies, $\Delta\omega$, between P^{*+} and $Q^{\bullet-}$, and the four transition frequencies are^{1,6,9,30}

$$\omega_1 \approx \omega_Q + J - d(\xi)$$

$$\omega_2 \approx \omega_P + J - d(\xi)$$

$$\omega_3 \approx \omega_Q - J + d(\xi)$$

$$\omega_4 \approx \omega_P - J + d(\xi)$$

where ω_Q and ω_P are the resonance positions of the two radicals, J is the exchange coupling, and $d(\xi)$ is the dipolar coupling, which is given by $d(\xi) = (D/3)(3 \cos^2 \xi - 1)$, with $D r_{PQ}^{-3} = -78.06 \text{ MHz} \cdot \text{nm}^3 = -2.786 \text{ mT} \cdot \text{nm}^3$ for point dipoles.⁹ r_{PQ} is the distance between the point dipoles, which, to a good approximation, can be positioned in the molecular centers of P^{*+} and $Q^{\bullet-}$. The distance vector between these centers defines the dipolar axis, z_d , and the angle, ξ , between z_d and the external magnetic field. It is important to note that the sign of $d(\xi)$ is orientation dependent. In the limit of slow molecular motion, each of $\omega_1 \dots \omega_4$ gives rise to a powder spectrum⁶ so that the total pattern of the pair $P^{*+}Q^{\bullet-}$ is the sum of four spin-polarized powder spectra. Two of the four spectra associated with $Q^{\bullet-}$ are referred [6] to as Q_{abs} and Q_{em} .

As shown previously,⁶ the two spectra closely resemble the powder spectrum of $Q^{\bullet-}$ because the coupling between the electrons is small compared to the anisotropy of the g -tensor. On the other hand, their sum is similar to the first derivative of Q_{abs} because the positions of the features in Q_{em} and Q_{abs} differ

slightly as a result of the weak splitting, δ , introduced by the coupling between the two electron spins. That is,

$$Q_{\text{em}}(B_0) \approx -Q_{\text{abs}}(B_0 + \delta)$$

The sum of the Q_{em} and Q_{abs} is then

$$Q_{\text{sum}}(B_0) \approx Q_{\text{abs}}(B_0) - Q_{\text{abs}}(B_0 + \delta)$$

which has the form of the first derivative of Q_{abs} . However, unlike the usual first derivative, the sign and magnitude of δ change across the spectrum. This affects the relative amplitudes and signs of the spectral features which occur at the three principal values of the quinone g -tensor. The sign of the polarization of the three features in the sum spectrum is directly related to the sign of the dipolar coupling, d , which is determined by the orientation of z_d relative to the three principal axes of $g(Q^{\bullet-})$ (x_Q , y_Q , and z_Q).

The W-band spectrum of $P_{700}^+ A_1^{\bullet-}$ (Figure 1, top (solid line)) can be interpreted qualitatively using the general features of the polarization pattern. From the emissive polarization on the low-field side of the spectrum it is clear that the angle between z_d and the x -axis of $g(A_1^{\bullet-})$ is small, which implies a large angle between z_d and the y - and z -axes. This is in contrast to the structural arrangement in Zn-bRCs, where the angle between z_d and the quinone y -axis is small and the angles between z_d and x and z are large. The high-field part of the spectrum consists of an A/E/A pattern. The absorptive feature on the left-hand side of this pattern indicates that the angle between z_d and the x -axis of $g(P_{700}^+)$ is large, as is also the case in Zn-bRCs. Care must be taken in interpreting the other features of the high-field part of the spectrum because of the overlap between the contribution from the z component of $g(Q^{\bullet-})$ and those from the y and z components of $g(P^+)$. Nonetheless, the close similarity of high-field parts of the PS I and Zn-bRC spectra and of the overall chromophore arrangement of the two RCs means that the relative orientation of z_d and $g(P^+)$ is similar in both systems.

Spectral Simulations. Having discussed the spectra qualitatively, we will now present the results of numerical simulations of the PS I spectrum. The calculations are based on the correlated coupled radical pair (CCRP) model, which is reviewed in refs 1 and 30. The assumptions contained in the model and its applicability to photosynthetic reaction centers have been discussed in ref 3. In Figure 2 simulations are shown in which as many independently determined parameters as possible have been used. Initially, the g -tensor of phylloquinone in frozen 2-propanol solution³² has been used for $g(A_1^{\bullet-})$. The g -tensor of P_{700}^+ has also been taken from independent experiments.³³ Recent measurements of the out-of-phase electron spin echo signal from $P_{700}^+ A_1^{\bullet-}$ ^{14,15} yield a reliable value of D (-0.170 ± 0.004 mT) and an upper limit of J (0.001 ± 0.0005 mT) for the dipolar and exchange couplings, respectively. The value of D yields a distance of 25.4 ± 0.3 Å between $A_1^{\bullet-}$ and P_{700}^+ in PS I, which is considerably shorter than the value of 28.4 ± 0.3 Å obtained for the distance between Q_{A^-} and P_{865}^+ . This result is also consistent with the transmembrane distances obtained from photovoltaic measurements,³⁴ which yield projections along the membrane normal. The hyperfine couplings are considered, in a first approximation, as contained in an inhomogeneous Gaussian linewidth. This leaves only the geometric parameters undetermined. On the basis of the qualitative analysis of PS I and bRC spectra (Figure 1), the orientation of z_d and $g(P_{700}^+)$ is taken to be the same as in bRCs. The orientation of A_1 is such that the x -axis of

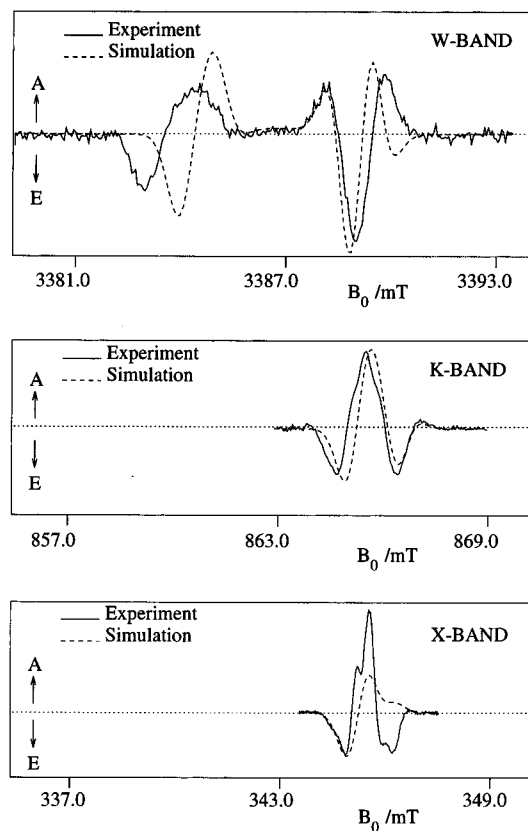


Figure 2. Simulation of the transient nutation EPR spectra of $P_{700}^+ A_1^{\bullet-}$ in PS I using parameters from the literature and in comparison with experimental spectra at three microwave frequencies. The parameters used are given in Table 1. For $A_1^{\bullet-}$, the principal g -values for phylloquinone in frozen solution³² have been used. The orientation of z_d relative to P_{700} has been assumed to be the same as that obtained from the X-ray structure⁴⁵ of bRCs of *Rb. sphaeroides*.

$g(A_1^{\bullet-})$ is parallel to z_d . The complete set of parameters is given in Table 1.

For these parameters, the quality of the simulations shown in Figure 2 is clearly not satisfactory. From the fact that the deviations on the low-field side of the spectra increase with increasing microwave frequency, it is obvious that the main reason for the poor agreement is that g_{xx} and g_{yy} must be larger for phylloquinone in PS I than in frozen 2-propanol solution. (that is, the low-field parts of the experimental spectra are shifted downfield compared to the simulations).

In Figure 2 (top) discrepancies are also observed in the high-field part of the W-band spectrum which cannot be attributed to the quinone g -tensor. The discrepancies are largest on the high-field end of the spectrum, which is determined by $g_{yy}(P^+)$ and $g_{zz}(P^+)$, whereas the agreement is quite good for the features corresponding to $g_{xx}(P^+)$. Thus, the orientation of the y - and z -axes of $g(P_{700}^+)$ may be somewhat different in PS I than in bRCs.

In Figure 3, a second set of simulated spectra is shown in which $g_{xx}(A_1^{\bullet-})$ and $g_{yy}(A_1^{\bullet-})$ have been adjusted to fit the positions of the spectral features. In addition, $g(P_{700}^+)$ has been rotated relative to z_d by 30° about its x -axis. (See Table 1). With this set of parameters, excellent agreement with the experimental W-band and K-band spectra is obtained. As expected, the simulation fails to reproduce the X-band spectrum. The main reason for the poor agreement is that the hyperfine couplings have only been taken into account in the form of an isotropic inhomogeneous Gaussian linewidth. At 9 GHz (X-band) the hyperfine couplings are a dominant contribution to the spectrum. Accordingly, the simulated spectra are very

TABLE 1: Simulation Parameters for $P_{700}^+A_1^{-}$

Magnetic Interaction Parameters			
<i>g</i> -tensors	g_{xx}	g_{yy}	g_{zz}
P_{700}^{+33}	2.0030	2.0026	2.0023
A_1^{-}	2.0062	2.0051	2.0022
VK_1^{+32}	2.0056	2.0049	2.0022
linewidth			
$\Delta B_{P_{700}} = 0.7$ mT			
$\Delta B_{A_1} = 0.7$ mT			
dipolar coupling ¹⁴	$D = -0.177$ mT		
exchange coupling ¹⁴	$J = 1.0$ μ T		
Orientational Parameters			
	α	β	γ
Euler angles ^a between the two <i>g</i> -tensors (Figure 2) ^b (Figure 3) ^c	75° 83°	158° 128°	0° 10°
	θ	ϕ	
polar angles describing z_d relative to <i>g</i> -tensor $Q^{\bullet-}$	90°	0°	

^a The transformation of $g(P^{+\bullet})$ from its principal axes to those of $g(Q^{\bullet-})$ is defined as follows: $g(P^{+\bullet}) = R(\alpha, \beta, \gamma) g(Q^{\bullet-}) R^T(\alpha, \beta, \gamma)$. The rotation matrix $R(\alpha, \beta, \gamma) = R_z(\gamma) R_y(\beta) R_x(\alpha)$ with

$$R_z(a) = \begin{pmatrix} \cos(a) & \sin(a) & 0 \\ -\sin(a) & \cos(a) & 0 \\ 0 & 0 & 1 \end{pmatrix}$$

$$R_y(a) = \begin{pmatrix} \cos(a) & 0 & -\sin(a) \\ 0 & 1 & 0 \\ \sin(a) & 0 & \cos(a) \end{pmatrix}$$

^b Assumed the same as in bRCs for the X-ray data reported in ref 45 and orientation II for $g(P_{865}^{+\bullet})$.⁴⁵ ^c Obtained by starting with the relative orientation of z_d and $g(P^{+\bullet})$ from bRCs and rotating $g(P^{+\bullet})$ by 30° about its *x*-axis.

sensitive to the assumed inhomogeneous linewidth. In particular, the fact that the orientation of the PS I RC with respect to the magnetic field is not resolved spectrally means that the orientation dependence of the couplings is a crucial factor. In recent ENDOR measurements on photoaccumulated A_1^{-} , a very large coupling which is assigned to the methylene protons of the phytyl chain has been observed.³⁶ In addition, the hyperfine couplings^{35,36} of the methyl protons at the 2-position on the quinone ring are quite anisotropic, with a large coupling in the direction of the principal *y*-axis of the *g*-tensor. Preliminary calculations suggest that this coupling is responsible for the partially resolved structure on the low-field side of the central absorption in the X-band spectrum. It is also possible that there is a distribution of orientations in the sample due to a distribution of protein environments, as suggested by the heterogeneous kinetics. However, we can rule this out as an important effect because the mosaic spread observed in X-ray studies would lead to, at most, minor effects in the spectra.

The good agreement of simulation and experiment at W-band and even K-band shows that the magnetic field dependent interaction parameters can be fixed well from the high-field results. This is an important precondition for a meaningful evaluation of the field independent parameters from further analysis of the low-field data. At present, it seems preferable to first determine the relative importance of other influences besides the hyperfine couplings. The linewidth contains contributions from relaxation, which is probably anisotropic³⁷ and can be determined independently with high-field experiments. In addition, spin dynamics in the precursor radical pair can also influence the polarization pattern (see ref 1). With the short lifetime (35 ps) of $P_{700}^+A_0^{\bullet-}$ this is likely to be irrelevant for PS I. Effects from coherent spin pair evolution at early times have to be separated as well. In conclusion, the

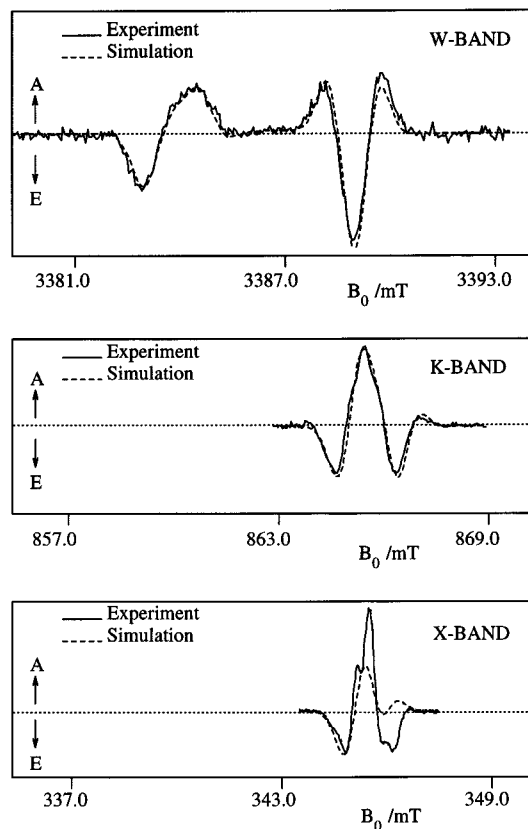


Figure 3. Simulation of the transient nutation EPR spectra of $P_{700}^+A_1^{-}$ in PS I using parameters that have been adjusted compared to those used in Figure 2. The *g*-values for A_1^{-} have been adjusted to $g_{xx} = 2.0062$, $g_{yy} = 2.0051$, $g_{zz} = 2.0022$. The *g*-tensor of P_{700} has been rotated relative to z_d and $g(A_1^{-})$ by 30° about its *x*-axis. All other parameters are the same as in Figure 2 (see Table 1).

large number of parameters has to be reduced by additional experiments before a meaningful simulation of the X-band spectra can be carried out.

Discussion

The most important results of the simulations in Figures 2 and 3 are (i) the anisotropy in the *g*-tensor of phyloquinone in the A_1 binding site in PS I is larger than that in frozen 2-propanol solution; (ii) A_1 is oriented such that its *x*-axis (C=O bond axis) is parallel to z_d . This orientation is very different from that of Q_A in bRCs.

In the following we will discuss these two results and their consequences for the A_1 binding site.

***g*-Tensor of A_1^{-} .** Analogous *g*-factor effects have been observed for duroquinone (DQ) and naphthoquinone (NQ), which show an even larger anisotropy increase when they are incorporated into PS I¹² in place of A_1 . In contrast, the *g*-anisotropy of $Q_A^{\bullet-}$ in bRCs shows only very small deviations from that of ubiquinone (UQ) in frozen 2-propanol solution,^{5,32,38} and no anisotropy change is observed with NQ and DQ.^{6,12}

As shown by Stone,^{39,40} the changes in the anisotropy of quinone *g*-tensors in different environments stem from the fact that mixing of the *n*- and π^* -orbitals due to spin-orbit coupling leads to a shift of g_{xx} and g_{yy} away from the free electron value. g_{zz} is unaffected because the *n*-orbitals are orthogonal to the *z*-direction. The larger anisotropy in PS I is due to stronger mixing of the orbitals most likely because $\Delta E_{n\pi^*}$ is smaller. This implies an increase in the energy of *n*-orbitals and/or a decrease in the energy of the π^* -orbitals.

There are several possible reasons why such a change in the orbital energies could occur. The most obvious of these is that

TABLE 2: Orientation of the P–Q Vector, z_d , Relative to the Principal Axes $g(P^{+\bullet})$ and $g(Q^{-\bullet})$

	$z_d, g(P^{+\bullet})$			$z_d, g(Q^{-\bullet})$		
	x_P	y_P	z_P	x_Q	y_Q	z_Q
PS I						
this work	76°	54°	39°	0°	90°	90°
ref 43	65°	55°	45°	0°	90°	90°
ref 10	60°	74°	35°	32°	91°	58°
bRCs ^a	76°	27°	68°	70°	28°	72°

^a The angles correspond to the X-ray data reported in ref 45 and orientation II for $g(P_{865}^{+\bullet})$.^{4,5}

different degrees of hydrogen bonding could exist in the various environments. Recent MO calculations [41, 42] of the g -tensors of quinone and tyrosine radicals show that the g -anisotropy increases with increasing hydrogen bond length. For bRCs, only subtle differences are observed in the g -factors of various quinones in the Q_A binding site and in frozen 2-propanol solution,^{12,38} which suggests that the effect of the hydrogen bonds in the two environments is rather similar. On the other hand, it has been shown that the hydrogen bonding of Q_A is asymmetric (see ref 2 for a summary), whereas in 2-propanol both oxygens are equally bonded. In addition, the orientation dependence of the T_2 relaxation measured at high field^{37,43} shows that there are marked differences in the angular librations of UQ in 2-propanol and bRCs. From this, it is clear that the relaxation behavior and the g -anisotropy are influenced differently by the surroundings. The g -tensor is a measure of the effect of the environment on the orbital energies and the spin density distribution, whereas the T_2 relaxation probes the potential energy surface, which determines the motion of the radical.

In contrast to bRCs, for which it is known that Q_A is hydrogen bonded to the protein,^{44,45} the nature of the binding of A_1 in PS I is not clear. The large anisotropy in $g(A_1^{-\bullet})$ suggests that the quinone binding is weaker in PS I than in bRCs. This notion is also supported by the fact that A_1 , NQ, and DQ have very different orientations in PS I, whereas in bRCs NQ and DQ all have essentially the same orientation^{12,46} as the native UQ. On the other hand, in recent ENDOR measurements^{35,36} of photo-accumulated $A_1^{-\bullet}$, substantial hyperfine couplings to exchangeable protons have been observed and were assigned to hydrogen bonds. If this assignment is correct, then the very different orientations of NQ and DQ mean that they cannot be bound to the protein in the same way as A_1 . It is possible that A_1 is bound via weak hydrogen bonds, whereas these are absent for the artificial acceptors NQ and DQ. This is consistent with the larger difference between the g -factors in frozen 2-propanol and PS I for NQ and DQ compared to A_1 (phylloquinone). An alternative explanation for the large g -anisotropy of all three quinones is that the orbital energies are shifted due to the Coulomb interactions with charged amino acid residues, as suggested to explain the g -anisotropy of the tyrosyl radicals in PS II⁴² and the redox potentials of iron–sulfur centers in various proteins.⁴⁷

Relative Orientation of $P_{700}^{+\bullet}$ and $A_1^{-\bullet}$. In Table 2 the orientation of z_d relative to the principal axes of two g -tensors $g(P^{+\bullet})$ and $g(Q^{-\bullet})$ is shown as used for the simulations in Figure 3. These angles also represent the orientation of the the g -tensors $g(P^{+\bullet})$ and $g(Q^{-\bullet})$ with respect to each other. Included in the table for comparison are the angles reported for PS I in perdeuterated cyanobacteria^{3,9–11,31} as well as those for bRCs.^{4,5} The values from refs 10 and 11 have been obtained from an analysis of the X-band transients and are based on the g -factors for phylloquinone in frozen solution, which, as we have shown here, are not valid for $A_1^{-\bullet}$. This is probably the main reason

for the differences between the two sets of angles for PS I. Not surprisingly, the largest differences occur in the relative orientation of z_d and $A_1^{-\bullet}$ ($\angle z_d, x_Q$ and $\angle z_d, z_Q$). Even if the correct g -factors are used, the angles from ref 10 do not reproduce the low field part of the W-band spectrum well.

As is evident from the W-band spectra in Figure 1 and the geometric parameters in Table 2, the orientation of the respective quinones A_1 and Q_A in PS I and bRCs is quite different. For P, on the other hand, the differences are relatively minor. As explained above, the difference between the two systems is that the angle between z_d and z_P is smaller, while the angle between z_d and x_P is the same. In bRCs, the z -axis of $P_{865}^{+\bullet}$ makes an angle of 22° with the average dimer normal^{4,48} and thus lies approximately in the membrane plane. The dipolar axis, on the other hand, lies close to the C_2 -axis and is thus nearly perpendicular to the membrane. The result is a value of $\sim 70^\circ$ for the angle between z_P and z_d . In contrast, this angle is 35–40° for PS I. This means that either (i) the z -axis of $g(P_{700}^{+\bullet})$ points further away from the normal to the porphyrin rings than in P_{865} , (ii) the porphyrin rings themselves are rotated closer to the membrane plane, (iii) the dipolar vector lies closer to the membrane plane, or some combination of i, ii, and iii. The second possibility can be ruled out on the basis of the latest X-ray⁸ and ENDOR⁴⁹ data, and although it is possible that the position of A_1 is such that z_d lies somewhat closer to the membrane plane in PS I than in bRCs, it is clear that it must be roughly perpendicular to the membrane in both systems. Thus, a difference in the orientation of the g -tensor axes relative to the molecular axes in P_{865} and P_{700} (possibility i) is probably the dominant effect.

A_1 Binding Site. If one compares the structure⁴⁵ of the electron carriers in bRCs with the electron density map⁸ of PS I, the following similarities with respect to position and orientation are observed for the two systems: (i) The donor P_{700} in PS I corresponds to the special pair P_{865} in bRCs, although the distance between the two chlorophyll planes is larger in P_{700} . (ii) The two chlorophylls labeled A and A' in ref 8 correspond to the two accessory chlorophylls in bRCs. (iii) The chlorophylls assigned to A_0 and A_0' in PS I correspond to the pheophytins in bRCs.

At present, the position of A_1 cannot be determined from the electron density map. However, A_1 should be found between A_0 and F_X . As a result, A_1 and A_1' are expected to lie near the stromal ends of helices e and e', which have been tentatively assigned⁵⁰ to transmembrane span 10, which is the second to last helix before the C-terminus in PsaA and PsaB. These helices probably also bind P_{700} via H680 in PsaA and H660 in PsaB on the luminal side as proposed in ref 50. This is supported by studies of mutants of *Chlamydomonas reinhardtii* in which the corresponding histidine H656 in PsaB was replaced by an asparagine.⁵¹ The mutants show a distinctly different ENDOR spectrum of $P_{700}^{+\bullet}$, indicating that H656 interacts with P_{700} . This part of the amino acid sequence⁵² is shown in Figure 4. In this region, there is a highly conserved section of the protein indicated by a shaded region. The fact that the only other motif in PsaA and PsaB, which is this strongly conserved, is the F_X binding region makes this section a good candidate for the A_1 binding site. If this part of the protein is indeed responsible for binding A_1 , then H708 (PsaA) and H688 (PsaB) are candidates for hydrogen bonding, whereas W706 and W697 (PsaA) and W686 and W677 (PsaB) could be involved in π type interactions with the quinone. The presence of charged residues in this region as shown in the figure could also account for the large anisotropy in the g -tensor, as indicated above. In light of the strong correlation between the redox potential of iron–sulfur centers and the number of neighboring charged

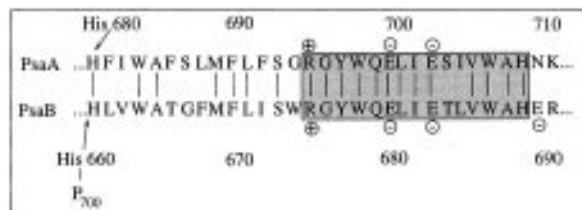


Figure 4. Section of the amino acid sequence of the PsaA and PsaB gene products in *S. elongatus* as reported in ref 52. The shaded area indicates a highly conserved region, which is a possible binding site for A_1 . The histidines H660 and H880 likely bind P_{700} (see ref 51 and text).

amino acid residues, which has recently been demonstrated,⁴⁷ it is conceivable that these residues also play a role in determining the redox potential of A_1 .

Concluding Remarks

We have shown that the anisotropy in the g -tensor of phylloquinone in the A_1 binding site in PS I is considerably different from that in frozen 2-propanol solution. This difference is explained by differences in the interaction of $A_1^{\bullet-}$ with its surroundings. In contrast to PS I, in bRCs only subtle effects are observed in this respect. This confirms earlier indications that the binding sites of the first quinone acceptors in the two systems are considerably different. This may also affect the mobility of the quinones. Here, high-field EPR experiments can provide additional information from the orientation dependence of the T_2 relaxation times obtained from the decay of the spin echo amplitude, as was demonstrated recently for chemically reduced $Q_A^{\bullet-}$ in bRCs and ubiquinone-10 in frozen solution.^{37,43} Similar experiments in PS I are in progress and will give further insight into the binding of A_1 .

Acknowledgment. We wish to thank M. Rohrer, J. Törring, and J. Claus for their contributions to the construction of the pulsed W-band EPR spectrometer. This work was supported by grants from the Deutsche Forschungsgemeinschaft (SFB 312, TP A1,A3,A4; and SFB 337, TP B3,B4) and Fonds der Chemischen Industrie (to W.L.).

References and Notes

- (1) Snyder, S. W.; Thurnauer, M. C. In *The Photosynthetic Reaction Center* Norris, J. R.; Deisenhofer, J., Eds.; Academic Press: New York, 1993; Vol. II, Chapter 11.
- (2) Angerhofer, A.; Bittl, R. *Photochem. Photobiol.* **1996**, *63*, 11.
- (3) Fuchsle, G.; Bittl, R.; van der Est, A.; Lubitz, W.; Stehlik, D. *Biochim. Biophys. Acta* **1993**, *1142*, 23.
- (4) van der Est, A.; Bittl, R.; Abresch, E.; Lubitz, W.; Stehlik, D. *Chem. Phys. Lett.* **1993**, *212*, 561.
- (5) Prisner, T.; van der Est, A.; Bittl, R.; Lubitz, W.; Stehlik, D.; Möbius, K. *Chem. Phys.* **1995**, *194*, 361.
- (6) van der Est, A.; Stehlik, D. In *Reaction Centers of Photosynthetic Bacteria*; Michel-Beyerle, M., Ed.; Springer: Berlin, 1995; Springer Series in Biophysics, p 321.
- (7) Ermler, U.; Fritsch, G.; Buchanan, S.; Michel, H. In *Research in Photosynthesis*; Murata, N., Ed.; Kluwer Academic Publishers: Dordrecht, 1992; Vol. I, p 341.
- (8) Schubert, W.; Klukas, O.; Krauss, N.; Saenger, W.; Fromme, P.; Witt, H. In *Photosynthesis: from Light to Biosphere*; Mathis, P., Ed.; Kluwer Academic Publishers: Dordrecht, The Netherlands, 1995; Vol. II, pp 3–10.
- (9) Stehlik, D.; Bock, C. H.; Petersen, J. *J. Phys. Chem.* **1989**, *93*, 1612.
- (10) Kothe, G.; Weber, S.; Ohmes, E.; Thurnauer, M. C.; Norris, J. R. *J. Phys. Chem.* **1994**, *98*, 2706.
- (11) Weber, S. Ph.D. Thesis, Universität, Stuttgart, 1994.
- (12) van der Est, A.; Sieckmann, I.; Lubitz, W.; Stehlik, D. *Chem. Phys.* **1995**, *194*, 349.
- (13) Krauss, N.; Hinrichs, W.; Witt, I.; Fromme, P.; Pritzkow, W.; Dauter, Z.; Betzel, C.; Wilson, K. S.; Witt, H. T.; Saenger, W. *Nature* **1993**, *361*, 326.
- (14) Bittl, R.; Zech, S. *J. Phys. Chem. B* **1997**, *101*, 1429.

- (15) Zech, S.; Lubitz, W.; Bittl, R. *Ber. Bunsen-Ges.* **1996**, *100*, 2041.
- (16) Witt, I.; Witt, H.; Gerken, S.; Saenger, W.; Dekker, J.; Rögner, M. *FEBS Lett.* **1987**, *221*, 260.
- (17) Fromme, P.; Witt, H. Manuscript in preparation.
- (18) Witt, H.; Krauss, N.; Hinrichs, W.; Witt, I.; Fromme, P.; Pritzkow, W.; Saenger, W. In *Proceedings of the IXth International Congress on Photosynthesis*; Nagoya Murata, N., Ed.; Kluwer Academic Publishers: Dordrecht, 1992; pp 521–528.
- (19) Prisner, T.; Rohrer, M.; Möbius, K. *Appl. Magn. Reson.* **1994**, *7*, 167.
- (20) Prisner, T. In *Advances in Magnetic and Optical Resonance*; Warren, W.; Ed.; Academic Press, New York, 1996; Vol. 20.
- (21) Bittl, R.; van der Est, A.; Kamrowski, A.; Lubitz, W.; Stehlik, D. *Chem. Phys. Lett.* **1994**, *226*, 349.
- (22) Stehlik, D.; Bock, C. H.; Thurnauer, M. C. In *Advanced EPR Applications in Biology and Biochemistry*; Hoff, A., Ed.; Elsevier: Amsterdam, 1989; Chapter 11, p 370.
- (23) Sétif, P.; Mathis, P.; Vänngård, T. *Biochim. Biophys. Acta* **1984**, *767*, 404.
- (24) Schlodder, E.; Brettel, K.; Falkenberg, K.; Gergeleit, M. In *Photosynthesis: from Light to Biosphere*; Mathis, P., Ed.; Kluwer Academic Publishers: Dordrecht, The Netherlands, 1995; Vol. II, pp 107–110.
- (25) Brettel, K. *FEBS Lett.* **1989**, *239*, 93.
- (26) Bock, C. H.; van der Est, A. J.; Brettel, K.; Stehlik, D. *FEBS Lett.* **1989**, *247*, 91.
- (27) Lüneberg, J.; Fromme, P.; Jekow, P.; Schlodder, E. *FEBS Lett.* **1994**, *338*, 197.
- (28) van der Est, A.; Bock, C.; Golbeck, J.; Brettel, K.; Sétif, P.; Stehlik, D. *Biochemistry* **1994**, *33*, 11789.
- (29) Moënné-Loccoz, P.; Heathcote, P.; MacLachlan, D.; Berry, M.; Davis, I.; Evans, M. *Biochemistry* **1994**, *33*, 10037.
- (30) Hore, P. J. In *Advanced EPR, Applications in Biology and Biochemistry*; Hoff, A., Ed.; Elsevier, Amsterdam, 1989; Chapter 12, p 405.
- (31) Weber, S.; Ohmes, E.; Thurnauer, M. C.; Norris, J. R.; Kothe, G. *Proc. Natl. Acad. Sci. U.S.A.* **1995**, *92*, 7789.
- (32) Burghaus, O.; Lubitz, W.; Plato, M.; MacMillan, F.; Rohrer, M.; Möbius, K. *J. Phys. Chem.* **1993**, *97*, 7639.
- (33) Prisner, T. F.; McDermott, A. E.; Un, S.; Norris, J. R.; Thurnauer, M. C.; Griffin, R. G. *Proc. Natl. Acad. Sci. U.S.A.* **1993**, *90*, 9485.
- (34) Hecks, B.; Wulf, K.; Breton, J.; Leibl, W.; Trissl, H.-W. *Biochemistry* **1994**, *33*, 8619.
- (35) Heathcote, P.; Rigby, S.; Evans, M. In *Photosynthesis: from Light to Biosphere*; Mathis, P., Ed.; Kluwer Academic Publishers: Dordrecht, The Netherlands, 1995; Vol. II, pp 163–166.
- (36) MacMillan, F.; Hanley, J.; Lubitz, W.; Rutherford, A. *Biophys. Biochim. Acta*, submitted.
- (37) Rohrer, M.; Gast, P.; Möbius, K.; Prisner, T. *Chem. Phys. Lett.* **1996**, *259*, 523.
- (38) Isaacson, R.; Abresch, E.; Feher, G.; Lendzian, F.; Lubitz, W. *Biophys. J.* **1995**, *69*, 311.
- (39) Stone, A. J. *Proc. R. Soc.* **1963**, *A271*, 424.
- (40) Stone, A. J. *Mol. Phys.* **1963**, *6*, 509.
- (41) Törring, J., Ph.D. Thesis, Institute for Experimental Physics, Free University, Berlin, 1996.
- (42) Un, S.; Atta, M.; Fontecave, M.; Rutherford, A. *J. Am. Chem. Soc.* **1995**, *117*, 10713.
- (43) Rohrer, M. Ph.D. Thesis, Institute for Experimental Physics, Free University, Berlin, 1996.
- (44) Chirino, A. J.; Lous, E.; Allen, J.; Schenck, C.; Feher, G.; Rees, D. C. *Biochemistry* **1994**, *33*, 4584.
- (45) Ermler, U.; Fritsch, G.; Buchanan, S.; Michel, H. *Structure* **1994**, *2*, 925.
- (46) van der Est, A.; Sieckmann, I.; Lubitz, W.; Stehlik, D. In *Photosynthesis: from Light to Biosphere*; Mathis, P., Ed.; Kluwer Academic Publishers: Dordrecht, The Netherlands, 1995; Vol. II, pp 143–146.
- (47) Banci, L.; Bertini, I.; Ciurli, S.; Luchinat, C.; Pierattelli, R. *Inorg. Chim. Acta* **1995**, *240*, 251.
- (48) Klette, R.; Törring, J.; Plato, M.; Bönigk, B.; Lubitz, W.; Möbius, K. *J. Phys. Chem.* **1993**, *97*, 2015.
- (49) Käss, H.; Fromme, P.; Witt, H. K.; Lubitz, W. *Biophys. J.* **1994**, *66*, A228.
- (50) Fromme, P.; Schubert, W.; Krauss, N. *Biochim. Biophys. Acta* **1994**, *1187*, 99.
- (51) Krabben, L.; Käss, H.; Schlodder, E.; Kuhn, M.; Lubitz, W.; Xu, H.; Bingham, S.; Webber, A. In *Photosynthesis: from Light to Biosphere*; Mathis, P., Ed.; Kluwer Academic Publishers: Dordrecht, The Netherlands, 1995; Vol. II, pp 123–126.
- (52) Mühlenhoff, U.; Haehnel, W.; Witt, H.; Herrmann, R. *Gene* **1993**, *127*, 71.